Soft Matter

Accepted Manuscript

ROYAL SOCIETY OF CHEMISTRY

www.rsc.org/softmatter

ARTICLE TYPE www. rsc.org/xxxxxx | XXXXXXXX

Dynamics of a liquid film of arbitrary thickness perturbed by a nano-object

Karol Wędołowski* and Marek Napiórkowski

Received Xth XXXXXXXXXX 20XX, Accepted Xth XXXXXXXXX 20XX
First published on the web Xth XXXXXXXXXX 200X
DOI: 10.1039/b000000x

We provide theoretical description of the dynamics of a liquid film perturbed by a nano-object. Our analysis is based on the general dispersion relation for surface perturbations which is valid for films of arbitrary thickness. In the case of thin liquid films the lubrication approximation is retrieved. The relevant time scales are derived and related to the characteristic length scales present in the system. We show that the multi length-scale character of the interfacial deformation is reflected in a wide range of the time scales describing the dynamics of the liquid film. In the case of relaxation under the action of a time-independent perturbation the analytical approximations to the interface evolution are obtained in several time regimes. The case of a general time-dependent perturbation is studied within the point-force approximation which allows to determine the universal aspects of liquid film dynamics. This method is also used to describe the response of the liquid film to a periodic perturbation which simulates the dynamic mode of the tip of atomic force microscope. It is shown that proper consideration of the thickness of the film leads to results which significantly differ from those obtained within the lubrication approximation even for relatively thin films.

1 Introduction

A substantial progress in experimental techniques devoted to the sub-micrometer measurements of liquid interfaces and solid surfaces has been taking place during the recent 20 years [1–3]. The atomic force microscope (AFM) plays a prominent role [2–4] in this field of research. It has been widely used in the study of surface properties of various materials including crystals, glasses, liquids, visco-elastic substances like polymers and lipid membranes, and colloidal particles [2,5,6]. Despite a growing number of applications of the AFM–related techniques there still exist difficulties with reliable control of the experimental conditions. A relevant issue concerns the spontaneous formation of a bridge between the AFM tip and the liquid layer located on top of the analysed solid surface [2–4,7–9]. This process can be triggered either by the capillary condensation [2,3,10,11] or by uncontrollable contact between the AFM tip and the liquid film [2,12–15]. The capillary condensation takes place in the ambient atmosphere, and - on the mesoscopic level of description - can be related to to the effective interaction of the liquid–gas interface with the tip and the substrate. On the other hand, the physical contact between the tip and the liquid film can be caused by both too large deflection of the AFM cantilever and the deformation of the liquid–gas interface caused by the long-range attractive forces (e.g. of van der Waals type). The motion of the cantilever can be controlled by increasing its spring constant or using the feedback mechanisms [2]. It is, however, much more difficult to control the deformation of the liquid interface. This aspect of the formation of capillary bridges has attracted much attention in recent years [12–20]. In particular, the minimum distance between the tip and the liquid–gas interface such that the liquid bridge is still absent has been analysed in several studies, [12–15,19,21] usually from the point of view of the equilibrium configurations of the interface. Recently Ledesma-Alonso et al. presented a detailed analysis [20] of the response of a thin liquid film to a periodically-varying perturbation which can be considered as a model of the interaction between a liquid film and the oscillating AFM tip working in the dynamic mode [22]. The authors show that the jump-to-contact event depends not only on the instantaneous distance between the tip and the liquid–gas interface but also on the frequency and the amplitude of tip oscillations. However, their analysis has been exclusively based on the thin liquid film (TLF) approximation, which has limited range of applications, e.g., with respect to micrometer-sized droplets.

In this paper we present a general theoretical and numerical study of the dynamics of a liquid film of arbitrary thickness perturbed by a nanosize object. We consider both the dynamics of the interface relaxing towards its equilibrium configuration and the interfacial dynamics resulting from periodic perturbations. In particular, we discuss the significance of different time scales appearing in the problem, and relate them

Institute of Theoretical Physics, Faculty of Physics, University of Warsaw, Pasteura 5, 02-093 Warszawa, Poland; E-mail: Karol.Wedolowski@fuw.edu.pl

to the appropriate length scales in the system. We investigate the general form of the dispersion relation of the interface perturbations which is valid for arbitrary thickness of the liquid film, and its asymptotic forms for very thick and very thin films. In particular, we investigate how the predictions of the asymptotic TLF theory deviate from the predictions based on the general approach as function of the film thickness and different time scales characterizing the perturbations. Also, we determine the regimes of time and length scales in which the predictions stemming from the TLF approximation turn out to be reliable.

2 Theory

2.1 Model

We consider a liquid film of infinite horizontal extent and thickness H. This uniform configuration is perturbed by a rigid sphere with radius R whose center is located at distance D from the unperturbed liquid–gas interface, see Fig. 1. In general, this distance may vary in time in a prescribed way given by $D(t)$. The deformation of the liquid–gas interface induced by the sphere is denoted by $\zeta(\mathbf{r},t)$, where $\mathbf{r}=(x,y)$ denotes the horizontal coordinates.

The interaction between the sphere and the film is described by the effective interface potential[23–25] $w(\mathbf{r},l(\mathbf{r},t))$, where the distance $l(\mathbf{r},t)=D(t)-\zeta(\mathbf{r},t)$ characterizes the relative position of the interface with respect to the actual position of the sphere, see Fig. 1. The corresponding disjoining pressure $\Pi(\mathbf{r},t)$ is related to the effective potential w[24,25] via

$$\Pi(\mathbf{r},t)=-\left.\frac{\partial w(\mathbf{r},\ell)}{\partial \ell}\right|_{\ell=D(t)-\zeta(\mathbf{r},t)} \quad . \tag{1}$$

Our analysis is focused on the attractive van der Waals interactions. Within the mean field theory (MFT) the disjoining pressure induced by the van der Waals interactions between the atoms of the sphere with its centre located at $\mathbf{r}=0, z=H+D$, and the atoms of the liquid film has the following form[12]

$$\Pi_p(\mathbf{r},t)=-\frac{4H_{pl}R^3}{3\pi}\left[(D(t)-\zeta(\mathbf{r},t))^2+r^2-R^2\right]^{-3} \quad , \tag{2}$$

where H_{pl} is the corresponding Hamaker constant, and $r=|\mathbf{r}|$ measures the radial distance from the symmetry axis. Negative values of the disjoining pressure reflect the attraction between the sphere and the liquid–gas interface. Obviously, the above form of the disjoining pressure does not take into account thermal fluctuations. To include them one has to go beyond the MFT, e.g., with the help of renormalization group theory[26] which leads to a modified version of Eq.(2)[27]. Our analysis is restricted to the mean field theory. In the case of thin liquid films the effective interface potential between the substrate–liquid and liquid–gas interfaces should be included into the general framework. The corresponding disjoining pressure $\Pi_w(\zeta(\mathbf{r}))$ has the following form

$$\Pi_w(\mathbf{r},t)=\frac{H_{sl}}{6\pi}\left[\frac{1}{(H+\zeta(\mathbf{r},t))^3}-\frac{1}{H^3}\right] \quad , \tag{3}$$

where H_{sl} is the relevant Hamaker constant. For $\zeta/H \ll 1$ one can use the linearised form of Π_w[15]

$$\Pi_w(\mathbf{r},t)=-\frac{H_{sl}}{2\pi H^4}\zeta(\mathbf{r},t) \; . \tag{4}$$

Also in this case, negative value of the disjoining pressure correspond to attraction between the substrate–liquid and liquid–gas interfaces.

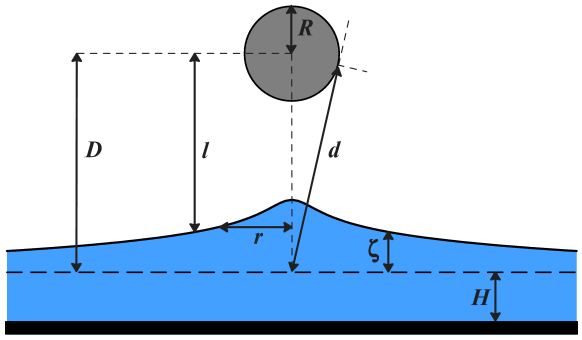

Fig. 1 A schematic plot of the system. The dashed line represents the reference level of the liquid–gas interface far away from the perturbed region. It corresponds to thickness H of uniform layer.

In this article we are mostly interested in dynamic response of liquid film to an external perturbation. However, for completeness, in the next subsection we present a short discussion of the relevant equilibrium properties of the liquid-gas interface induced by static perturbations.

2.2 Equilibrium profiles of the liquid–gas interface

In equilibrium, the shape of the liquid–gas interface interacting with a planar substrate and a sphere, see Fig. 1, is governed by the generalized Young-Laplace equation[12–15]

$$2\kappa\gamma+\Pi_p=\Pi_w-\Delta\rho\, g\,\zeta \quad , \tag{5}$$

where κ is the mean curvature of the interface, γ is the coefficient of the liquid–gas surface tension, g is the gravitational acceleration, and $\Delta\rho=\rho_l-\rho_g$ is the difference between the liquid and gas mass densities. The problem has cylindrical symmetry and therefore we write the mean curvature as a function of the radial distance $r=|\mathbf{r}|$

$$2\kappa=-\frac{1}{r}\frac{\partial}{\partial r}\left[r\frac{\partial\zeta}{\partial r}\left\{\left(\frac{\partial\zeta}{\partial r}\right)^2+1\right\}^{-1}\right] \tag{6}$$

which for smooth interfacial configurations $|\partial\zeta/\partial r| \ll 1$ [12–15], becomes

$$2\kappa \approx -\frac{\partial^2\zeta}{\partial r^2} - \frac{1}{r}\frac{\partial\zeta}{\partial r} \,. \tag{7}$$

This leads to the following equation for the interfacial profile

$$-\frac{\partial^2\zeta}{\partial r^2} - \frac{1}{r}\frac{\partial\zeta}{\partial r} + \zeta\left(\frac{1}{\lambda_c^2} + \frac{1}{\lambda_w^2}\right) = \frac{4H_{pl}R^3}{3\gamma\pi}\left[(D-\zeta)^2 + r^2 - R^2\right]^{-3} \,, \tag{8}$$

which depends on the capillary length $\lambda_c = \sqrt{\gamma/(\Delta\rho g)}$ and the length scale $\lambda_w = \sqrt{2\pi\gamma H^4/H_{ls}}$ related to the effective substrate–liquid interaction. In our analysis this interaction plays similar role to the gravitational potential and both lengths can be incorporated into the *effective* capillary length $\lambda = \left(\lambda_c^{-2} + \lambda_w^{-2}\right)^{-1/2}$ [15]. For the Hamaker constants of the order of 10^{-19} J [28] and the surface tension coefficient of the order of 10 mJ/m^2 one obtains $\lambda_w \sim H^2\, 10^9$ m^{-1}. Thus for realistic value of the capillary length $\lambda_c \approx 10^{-3}$ m the effect of the substrate–liquid interaction can be neglected for $H \gtrsim 10^{-6}$ m. On the other hand for much thinner films the effective capillary length is determined solely by the length scale λ_w.

Equation(8) is accompanied by two boundary conditions

$$\left.\frac{\partial\zeta}{\partial r}\right|_{r=0} = 0 \,, \tag{9}$$

$$\zeta(r) = 0 \;\text{ for } r \to \infty \tag{10}$$

which reflect the cylindrical symmetry of the system and make the distortion of the locally perturbed interface to vanish at infinity. Actually, the asymptotic analysis [14] of Eq.(8) estimates the linear size of this distorted region to be of the order of the effective capillary length. Eq.(8) can be solved numerically with the help of the shooting method. Using the dimensionless variables $r' = r/R$, $D' = D/R$, $H' = H/R$, and $\zeta' = \zeta/R$, Eq.(8) takes the form

$$-\frac{\partial^2\zeta'}{\partial r'^2} - \frac{1}{r'}\frac{\partial\zeta'}{\partial r'} + \tilde{B}_o\zeta' = -\Pi_p' \,, \tag{11}$$

where

$$\Pi_p'(r') = -\frac{H_a}{\left[(D'-\zeta'(r'))^2 + r'^2 - 1\right]^3} \tag{12}$$

is the dimensionless disjoining pressure, $H_a = 4H_{pl}/(3\gamma\pi R^2)$, and $\tilde{B}_o = R^2/\lambda^2$ is the effective Bond number which depends on H via λ_w. For $H_{pl} = H_{sl}$ the effective Bond number can be written as

$$\tilde{B}_o = B_o + \frac{3H_a}{8H'^4} \,, \tag{13}$$

where $B_o = R^2/\lambda_c^2$. Later on we shall use the values $H_a = 10^{-3}$ and $B_o = 10^{-10}$, which correspond to the radius of the sphere of the order of tens of nanometres.

A detailed analysis of the solutions of Eq.(11) has already been presented in the literature [12,13,15]. In particular, Ledesma-Alonso et al. [12,13] have determined the minimum value D_{min} for which the capillary bridge is still absent. This distance depends on H_a but is almost insensitive to changes of $\tilde{B}_o$. The equilibrium profiles of the liquid–gas interface obtained numerically from Eq.(11) for $H_a = 10^{-3}$, $\tilde{B}_o = 10^{-10}$ and different values of the distance D' are shown on Fig.2. In this case one has $D'_{min} \approx 1.168$.

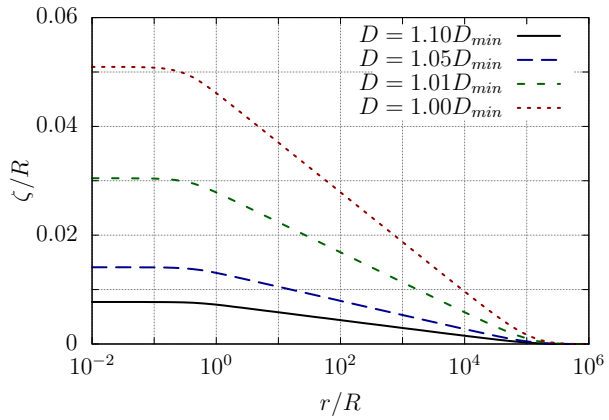

Fig. 2 Numerical solutions of Eq.(11) for $\tilde{B}_o = 10^{-10}$, $H_a = 10^{-3}$, and different values of the distance D. The scale of the horizontal axes is logarithmic.

From Eq.(12) one can deduce that the deformation of the interface has negligible impact on the values of the disjoining pressure if $\zeta/\varepsilon \ll 1$, where $\varepsilon = D - R$ is the separation between the surface of the tip and the non-perturbed position of the liquid–gas interface. In such case Eq.(11) reduces to

$$-\frac{\partial^2\zeta'}{\partial r'^2} - \frac{1}{r'}\frac{\partial\zeta'}{\partial r'} + \tilde{B}_o\zeta' = \frac{H_a}{\left[d'^2 + r'^2\right]^3} \,, \tag{14}$$

where $d'^2 = D'^2 - 1$. The geometrical interpretation of the quantity $d = d'R$ is presented in Fig.1. Approximate analytical solutions to Eq.(14) can be found by considering its asymptotic forms for $r' \sim 1$ and $r' \sim \tilde{B}_o^{-1/2}$ and matching them in the intermediate region [14]. This procedure gives

$$\zeta'(r') = \frac{H_a}{4d'^4}\left\{\frac{1}{2}\ln\left(\frac{r'^2}{d'^2 + r'^2}\right) + \frac{1}{2}\frac{d'^2}{d'^2 + r'^2} + K_0\left(\tilde{B}_o^{1/2}\, r'\right)\right\} \,, \tag{15}$$

where K_0 denotes the zeroth–order modified Bessel function of the second kind. These analytical solutions are presented in Fig. 3 for the same values of D as in Fig. 2.

One concludes that the exact solutions can be represented by the approximate expressions in Eq.(15) only for $D \gtrsim$

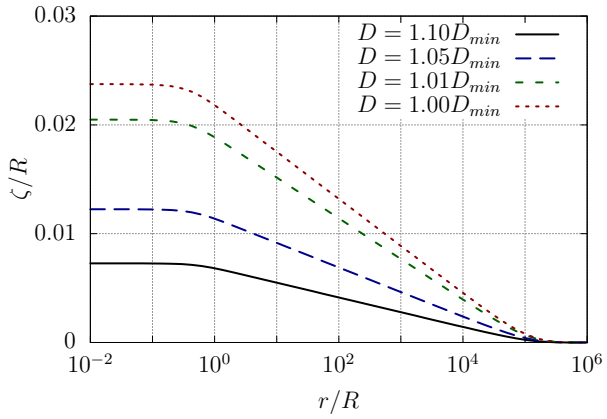

Fig. 3 Approximate analytical solutions of Eq.(14) for $\tilde{B}_o = 10^{-10}$, $H_a = 10^{-3}$, and different values of the distance D. The scale of the horizontal axes is logarithmic.

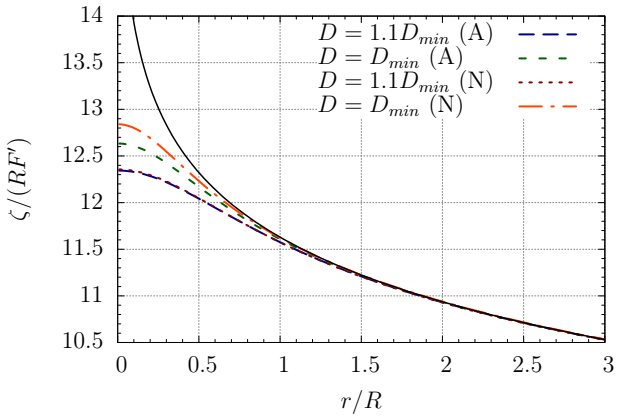

Fig. 4 Liquid–gas interface profiles normalized by RF' have been obtained using the analytical formula (A) and the numerical scheme (N). The solid line represents the interface profile corresponding to the point force, $\Pi_p(\mathbf{r}) = F\delta(\mathbf{r})$.

$1.1D_{min}$. For smaller values of D, the relative difference between the exact and approximate solutions increases significantly, up to about 50% for D approaching D_{min}.

One important consequence of a small value of the Bond number is that the shape of the liquid–gas interface is directly influenced by the disjoining pressure only in a relatively small region corresponding to $r \lesssim d$. Outside this region the interface deformation is independent of the actual disjoining pressure distribution and depends only on the total force exerted on the interface. Similar observation have already been presented by Chan et al.[18] in the context of the dynamic deformation of droplets and bubbles. Figure 4 shows profiles - obtained both numerically (N) and analytically (A) - normalized by the dimensionless total force

$$F' = \frac{F}{2\pi\gamma R} = -\int_0^\infty r'\Pi(r')\mathrm{d}r' \,. \tag{16}$$

Note that in the analytical calculation of the profiles we used the approximate disjoining pressure from Eq.(14) which gives $F' = H_a/(4d'^4)$. This conclusion will be particularly important in the description of the time evolution of the interface presented in the following sections.

2.3 Dynamics of liquid film

From the macroscopic point of view the time evolution of the liquid film brought about by external perturbation is described by the incompressible Navier-Stokes equations with the appropriate set of boundary conditions[29,30]. Our analysis is based on the linearised Navier-Stokes equations

$$\frac{\partial \mathbf{u}}{\partial t} = -\nabla\left(\frac{p}{\rho_l}\right) - g\mathbf{e_z} + \nu\nabla^2\mathbf{u} \,, \tag{17}$$

$$\nabla\cdot\mathbf{u} = 0 \,, \tag{18}$$

where $\mathbf{u}$ is the velocity field, p denotes the pressure, ν is the coefficient of kinematic viscosity, and $\mathbf{e_z}$ is a unit vector in direction perpendicular to the substrate. The following linearised boundary conditions are imposed on the liquid film

$$\mathbf{u} = 0 \quad \text{at } z = 0 \,, \tag{19}$$

$$u_z = \frac{\partial \zeta}{\partial t} \quad \text{at } z = H \,, \tag{20}$$

$$\frac{\partial u_x}{\partial z} + \frac{\partial u_z}{\partial x} = 0 \quad \text{at } z = H \tag{21}$$

$$\frac{\partial u_y}{\partial z} + \frac{\partial u_z}{\partial y} = 0 \quad \text{at } z = H \tag{22}$$

$$\left(p - 2\rho_l\nu\frac{\partial u_z}{\partial z}\right) + \Pi_w(\mathbf{r},t) = -\gamma\left(\frac{\partial^2\zeta}{\partial x^2} + \frac{\partial^2\zeta}{\partial y^2}\right) + \Pi_p(\mathbf{r},t) \quad \text{at } z = H \,. \tag{23}$$

Equation (19) represents the no-slip boundary condition at the substrate surface. Equation (20) expresses the linearised kinematic boundary condition at the liquid–gas interface. It ensures that the mass flux through the interface is equal to zero. For non-critical states considered in this paper the dynamic viscosity of the liquid phase is much larger than that of the gas, and the shear stresses can be neglected at the interface. This condition is represented in Eqs(21,22). On the other hand the difference between the normal stresses on both sides of the interface has to be equal to the Laplace pressure which is related to the interface curvature. This fact is reflected in Eq.(23). The boundary conditions at the liquid–gas interface are, in fact, imposed at the surface $z = H$ and not at $z = H + \zeta$. This is the consequence of the linearisation procedure in which the value of any field evaluated at $z = H + \zeta$ can be expanded around

$z = H$ in Taylor series.

On the other hand, the disjoining pressure term in Eq.(23) has not been linearised. The reason for this is that the disjoining pressure, Eq.(2), depends on the deformation ζ via the ratio ζ/ε which may not be negligible even if the deformation itself is small enough to be described by the linearised dynamics. In this case we consider the disjoining pressure as an *á priori* unknown function of r and t.

A short discussion of boundary conditions which are different from those used in this paper, and their influence on the results, in particular the dispersion relation, see Eq.(31) below, can be found in Appendix A.

By applying the Fourier analysis to Eqs(17-23) one obtains the following equation for the Fourier transform $\hat{\zeta}(k,\omega) = \int d\mathbf{r} \int dt \, \exp(-i\mathbf{k}\cdot\mathbf{r} - i\omega t)\, \zeta(\mathbf{r},t)$ of the liquid–gas interface deformation [31]

$$\left(\frac{k}{\lambda^2} + k^3 - \frac{\rho_l}{\gamma}\Omega^2(k,\omega)\right)\hat{\zeta}(k,\omega) = -\frac{k\hat{\Pi}_p(k,\omega)}{\gamma} \,, \quad (24)$$

where $\hat{\Pi}_p(k,\omega)$ is the Fourier transform of $\Pi_p(\mathbf{r},t)$, which we assumed to be axisymmetric. The function $\Omega^2(k,\omega)$ is given by the following expression [31]

$$\Omega^2(k,\omega) = 4\nu^2\left(\tilde{\alpha}^4\tilde{B} - k^3\alpha\tilde{D}\right) \,, \quad (25)$$

where

$$\tilde{B} = \frac{1}{M - \frac{k}{\alpha}\frac{QL}{W}}\left[L - \frac{k}{\alpha}\frac{QM}{W} - \frac{k^2}{\tilde{\alpha}^2}\frac{1}{W}\right] \,, \quad (26)$$

$$\tilde{D} = \frac{1}{Q}\left[W - \frac{\tilde{\alpha}^2}{k^2}\left(L - \tilde{B}M\right)\right] \,, \quad (27)$$

$$\alpha^2 = k^2 + \frac{i\omega}{\nu} \,,\ \tilde{\alpha}^2 = k^2 + \frac{i\omega}{2\nu} \,, \quad (28)$$

and $L = \cosh(kH)$, $M = \sinh(kH)$, $W = \cosh(\alpha H)$, $Q = \sinh(\alpha H)$.

The shape $\zeta(r,t)$ of the liquid–gas interface is obtained by inverting both the temporal and the spatial Fourier transforms. The integration over ω can be performed analytically only in special cases, e.g., when the perturbing object moves horizontally with a constant velocity [31]. Also, in situations when the dimensionless parameter

$$\mathscr{R}_{k,\omega} = \left|\frac{\omega}{\nu k^2}\right| \,, \quad (29)$$

is either very small or infinitely large the implicit dispersion dispersion relation

$$\frac{k}{\lambda^2} + k^3 - \frac{\rho_l}{\gamma}\Omega^2(k,\omega) = 0 \,, \quad (30)$$

can be solved for $\omega = \omega(k)$. As a consequence, one obtains the differential evolution equation for $\hat{\zeta}(k,t)$. The case of an infinite values of $\mathscr{R}_{k,\omega}$ was analysed by Closa et al. [32]. Here we discuss the case of $\mathscr{R}_{k,\omega} \ll 1$ which is suitable for nanoscopic problems.

In this limit the dispersion relation, Eq.(30), takes the form

$$\frac{k}{\lambda^2} + k^3 + 2i\frac{\mu}{\gamma}\omega k^2 g(kH) = 0 \,, \quad (31)$$

where $\mu = \rho_l\nu$ is the coefficient of dynamic viscosity, and

$$g(x) = \frac{\cosh^2(x) + x^2}{\sinh(x)\cosh(x) - x} \,. \quad (32)$$

As a result, the integration of Eq.(24) over ω leads to the following evolution equation

$$2\frac{\mu}{\gamma}k^2 g(kH)\frac{\partial}{\partial t}\hat{\zeta}(k,t) + \left(\frac{k}{\lambda^2} + k^3\right)\hat{\zeta}(k,t) = -\frac{k\hat{\Pi}_p(k,t)}{\gamma} \,. \quad (33)$$

In the limit of thin liquid films, the above equation reduces to the equation obtained by Ledesma-Alonso et al. [20]. Thus Eq.(33) can be considered as a generalization of their results to films of arbitrary thickness.

The general solution to Eq.(33) has the following form

$$\hat{\zeta}(k,t) = \left\{\hat{\zeta}(k,0) + \right. \quad (34)$$
$$\left. - \int_0^t \left[\frac{\hat{\Pi}_p(k,\tau)}{2\mu k g(kH)} e^{\Gamma(k)\tau}\right] \mathrm{d}\tau\right\} e^{-\Gamma(k)t} \,,$$

where

$$\Gamma(k) = \frac{\gamma}{2\mu}\frac{1}{g(kH)}\left(k + \frac{1}{k\lambda^2}\right) \quad (35)$$

is the decay rate given by the imaginary part of the frequency obtained from Eq.(31), and $\hat{\zeta}(k,0)$ denotes the Fourier transform of the initial surface profile. In the **r**-space, this solution can be written as

$$\zeta(r,t) = 2\pi\int_0^\infty k\hat{\zeta}(k,0)e^{-\Gamma(k)t}J_0(kr)\mathrm{d}k + \quad (36)$$
$$- 2\pi\int_0^\infty\int_0^t \left[\frac{\hat{\Pi}_p(k,t-\tau)}{2\mu k g(kH)} e^{-\Gamma(k)\tau}\right]\mathrm{d}\tau J_0(kr)\mathrm{d}k \,.$$

where J_0 is the zeroth-order Bessel function of the first kind. The first term on the rhs of Eq.(36) represents the evolution of the initial profile according to the dispersion relation. It vanishes for initially flat interface. The second term describes the response of the liquid film to the disjoining pressure acting on the interface. This response is not instantaneous and the dispersion relation provides different scales of „memory" for different wave numbers. Note that in a general case Eq.(36) cannot be considered as an explicit formula for $\zeta(r,t)$ since the disjoining pressure also depends on the interface deformation. Nevertheless, this formal expression, turns out to be helpful in

understanding the general aspects of the interface response to the external perturbation, which is presented in Sec. 3.2. In the next subsection we discuss the various time scales relevant to our problem.

2.4 Dispersion relation and relevant time scales

The dispersion relation in Eq.(31) was obtained under the assumption $\mathscr{R}_{k,\omega} \ll 1$. One should check whether this approach is self-consistent. After substituting the ω obtained from Eq.(31) to the definition of $\mathscr{R}_{k,\omega}$ in Eq.(29) one obtains the following condition

$$\frac{\gamma\lambda_c}{2\rho\nu^2}\,\frac{(k^2\lambda_c^2+(\lambda_c/\lambda)^2)}{k^3\lambda_c^3 g(k\lambda_c\cdot H/\lambda_c)} \ll 1\,. \tag{37}$$

The first fraction on the lhs is a liquid-dependent number, e.g. of order 1 for the silicon oil, 10^4 for liquid hydrocarbons, and 10^5 for water at room temperature. The second fraction is a function of the dimensionless wave number $k\lambda_c$ and the thickness of the liquid film H/λ_c. In Fig.5 a typical dependence of $\mathscr{R}_{k,\omega}$ on the dimensionless wave number for different thicknesses of the liquid film is presented for the case of liquid hydrocarbons. For such systems the low $\mathscr{R}_{k,\omega}$ approximation is adequate for arbitrary k provided $H \ll 10^{-4}\lambda_c$. And, for $k\lambda_c \gg 10^4$ this approximation can be used for films of arbitrary thickness. On the other hand, for small wave numbers and films of the thickness $H/\lambda_c \in [10^{-4}, 10^{-2}]$ the condition $\mathscr{R}_{k,\omega} \ll 1$ is satisfied only for $k \ll 1/H$. This can be seen from Fig. 5 if one notes that the maximum of each curve is located at $k \sim 1/H$.

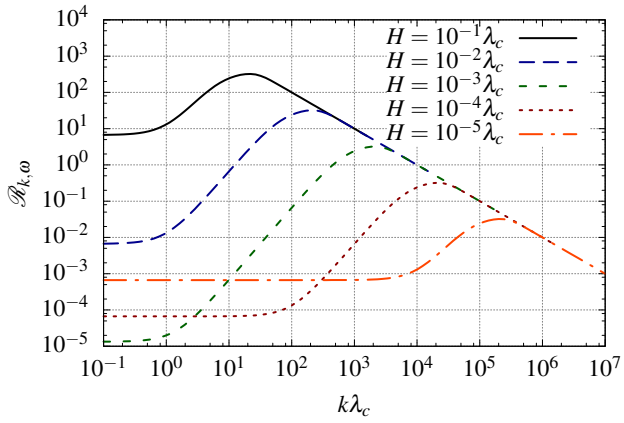

Fig. 5 The parameter $\mathscr{R}_{k,\omega}$ as a function of dimensionless wave number $k\lambda_c$, Eq.(37), for typical liquid hydrocarbons at room temperature: $\gamma = 0.02$ N/m, $\rho = 800$ kg/m^3, $H_{ls} = 10^{-19}$ J, $\nu = 10^{-6}$ m^2/s, and for different values of the dimensionless film thickness H/λ_c.

Three different regions of wave numbers can be distinguished in Fig. 5. In each of them the dispersion relation and parameter $\mathscr{R}_{k,\omega}$ behave in a different way. For very small wave numbers the parameter $\mathscr{R}_{k,\omega}$ is constant. This is caused by the approximately quadratic nature of the dispersion relation. The size of this region is bounded by the inverse of the effective capillary length, which is equal to λ_c for relatively thick films. For thinner films λ decreases for decreasing H and consequently the region of constant $\mathscr{R}_{k,\omega}$ spans a wider range of wave numbers. For $1/\lambda \ll k \ll 1/H$ the parameter $\mathscr{R}_{k,\omega}$ grows upon increasing $k\lambda_c$ because the dispersion relation becomes a quartic function of the wave number. This regime of the liquid film dynamics is well described by the TLF approximation[31,33], in agreement with the asymptotic form of the decay rate

$$\Gamma(k) \approx \Gamma_{TLF}(k) = \frac{\gamma}{3\mu}(kH)^3\left(k+\frac{1}{k\lambda^2}\right) \quad \text{for } kH \ll 1\,. \tag{38}$$

On the other hand, for $k \gg 1/H$ one observes a universal character of $\mathscr{R}_{k,\omega}$. It is caused by the linear form of the dispersion relation, independent of H, and described by the infinite thickness approximation

$$\Gamma(k) \approx \Gamma_{\infty}(k) = \frac{\gamma}{2\mu}\left(k+\frac{1}{k\lambda^2}\right) \quad \text{for } kH \gg 1\,. \tag{39}$$

For a given wave number the decay rate determines the characteristic relaxation time $\tau(k) = 1/\Gamma(k)$, which, in turn, can be related to the characteristic length scale. There are four natural length scales in our problem: the sphere radius R, the distance D between the sphere and the reference interface position, the effective capillary length λ, and the film thickness H. They determine the relevant wave numbers. The wave number $k_\lambda = 1/\lambda$ gives the lower bound on the deformation spectrum. On the other hand, the determination of the upper bound is a subtle issue. It can be resolved by investigating the Fourier transform of the disjoining pressure. In general, the disjoining pressure depends on the surface profile but for small deformations $\zeta/\varepsilon \ll 1$ the approximate upper bound $k_d = 1/d$ can be obtained. It increases for decreasing both D and R, but for distances analysed in this study it remains numerically close to $k_R = 1/R$. On the other hand for significant surface deformations, close to the bridge formation, the upper bound of the spectrum shifts towards larger wave numbers[20]. Although, this can be hardly determined analytically, the analysis of the equilibrium surface profiles shows that even for the maximum deformation the wave number k_d is a reasonable estimate of the upper cutoff. The corresponding characteristic time scales are denoted $\tau_\lambda = \tau(k_\lambda)$ and $\tau_d = \tau(k_d)$. For $R \ll H \ll \lambda$ they can be obtained from the asymptotic expressions for the decay rate, i.e., from Eqs (38,39)

$$\tau_\lambda \approx 3\tilde{B}_o^{-2}\left(\frac{H}{R}\right)^{-3}\tau_0\,, \quad \tau_d \approx 2\frac{d}{R}\tau_0\,, \tag{40}$$

where $\tau_0 = R\mu/\gamma$. These two time scales can differ significantly and their ratio depends on the relation between the length scales λ, H, R and d.

The time scale τ_λ governing the relaxation of long-wavelength perturbations plays an essential role in the deformation dynamics at $r \sim \lambda$. On the other hand, τ_d determines the relaxation time for the region of the interface for which $r \lesssim d$, the so-called near-field deformation of the interface.

The length scale H plays another important role in the dynamics of the liquid film. The corresponding wave number $k_H = 1/H$ splits the Fourier space into two regions in which the dynamics is determined by two asymptotic forms of the dispersion relation. The time scale $\tau_H = \tau(k_H)$ can be approximated by

$$\tau_H = 2g(1)\tau_0 \frac{H}{R} \approx 8\tau_0 \frac{H}{R} \,. \qquad (41)$$

In the following sections we show that if the characteristic time scale of the perturbation is smaller than τ_H then the response of the liquid film is given by the infinite thickness approximation. On the other hand, the TLF dynamics characterizes the surface deformation on time scales much larger than τ_H.

In order to estimate the time and length scales in typical experiments one has to provide values of the relevant parameters present in the problem. The radius of of the AFM tip can vary from ~ 10 nm to ~ 1 μm, the latter referring to the colloidal probe AFM. The dynamic viscosity coefficient spans a range of 10^{-3} to 10^{-1} Pa·s, while the surface tension coefficient has values between 10^{-3} and 10^{-2} J/m^2. Consequently, one obtains $\tau_0 \in [10^{-9} - 10^{-4}$ s]. In the non-contact AFM experiments the cantilever can oscillate with the frequency ranging from 10^4 to 10^6 Hz, while it does not oscillate at all in the force spectroscopy experiments with the colloidal probe AFM[2]. In the latter case the characteristic time scale depends on the velocity at which the probe approaches the sample.

3 Results

3.1 Time-independent perturbation

We begin the analysis of different time scales introduced in the previous section by considering the special case of the ζ–independent disjoining pressure

$$\Pi_0(r) = \Pi_p(r, \zeta = 0) = -\frac{4H_{pl}R^3}{3\pi\gamma} \left[d^2 + r^2\right]^{-3} \,. \qquad (42)$$

Its Fourier transform in dimensionless variables introduced in Sec. 2.2 takes the following form

$$\hat{\Pi}_0'(k') = \frac{\hat{\Pi}_0(k'/R)}{2\pi\gamma R} = -\frac{F'}{2}(k'd')^2 K_2(k'd') \,. \qquad (43)$$

If the distance D does not depend on time the integral in Eq.(36) can be evaluated analytically and for initially planar interface $\zeta(r, t = 0) = 0$ one obtains

$$\zeta'(r', t') = \frac{F'}{2} \int_0^\infty \frac{k'(k'd')^2 K_2(k'd')}{k'^2 + \tilde{B}_o} \left[1 - e^{-\Gamma'(k')t'}\right] J_0(k'r') \mathrm{d}k' \,, \qquad (44)$$

where $t' = t/\tau_0$ and

$$\Gamma'(k') = \tau_0 \Gamma(k'/R) = \frac{1}{2\,g(k'H')} \left(k' + \frac{\tilde{B}_o}{k'}\right) \,. \qquad (45)$$

The integral in Eq.(44) was calculated numerically using the Simpson rule implemented in the Octave[34] environment. We have chosen this simple numerical method because the strongly oscillating integrand in Eq.(44) requires a fine spatial discretization in the whole integration domain and, consequently, different adaptive quadratures do not bring much benefit. All results presented in this section correspond to the choice $H_a = 10^{-3}$ and $B_o = 10^{-10}$. Time is expressed in the units τ_0.

In Fig. 6 we show the shape of the interface at different times for $H = 100R$ and $D/D_{min} = 1.1$. These results were obtained within three different approaches, each characterized by the corresponding decay rate discussed in the previous section. One observes a multi-scale temporal evolution of the interface. The plot (a) presents the predictions of the general theory, Eq.(35). At $t \approx \tau_0 \sim \tau_d$ the deformation of the interface is confined to the region $r \lesssim 10R$ and attains not more than approximately 10% of its final magnitude. The mechanical equilibrium is reached at $t \approx 10^{14}\tau_0 \sim t_\lambda$. One can compare these results to the asymptotic time evolution in two special cases: (b) $kH \to 0$, and (c) $kH \to \infty$. For $H = 100R$ we have $\tau_H = 800\tau_0$. One concludes that indeed the TLF approximation is adequate for $t \gg \tau_H$ but it fails to describe the initial stage of the interface evolution. The TLF approximation underestimates the relaxation time of the interface for $r \ll H$. This is related to significantly higher value of the decay rate for $k \gg k_H$ observed within this approximation as compared to the general theory. On the other hand, the approximation of infinitely thick film works well only for times $t \ll \tau_H$ and underestimates the relaxation time for $r \gg H$.

One observes that the shape of the inner part of the profiles ($r \lesssim d$) becomes equilibrated already at $t \sim \tau_d$ and then does not change in the course of time except for being lifted, as the rest of the interface grows. This can be understood by realizing that the wave numbers responsible for the shape of the inner profile correspond to $k \gtrsim 1/d$ and, consequently, equilibrate at $t \sim \tau_d$. Smaller wave numbers set the absolute position of the near-field deformation only.

As already discussed in Sec. 2.2 the interface deformation normalized by the total force exerted on the interface depends

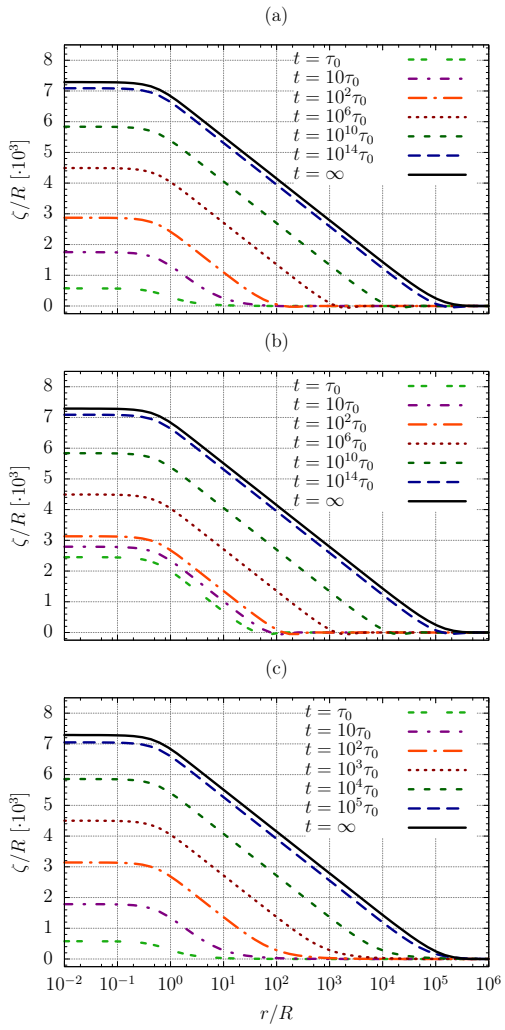

Fig. 6 The transient profiles of the interface given by Eq.(44) for $H = 100R$ and $D = 1.1D_{min}$ obtained using (a) the general dispersion relation, (b) the TLF approximation, and (c) the infinite thickness approximation.

on the distance D only in the inner region $r \lesssim d$. Similarly, the normalized transient profiles obtained for different distances between the probe and the interface are very close to each other. Small differences between the inner parts of the profiles are already visible at $t \sim \tau_d$ and remain unchanged during the time evolution. This can be observed in Fig. 7 where the normalized apex position, i.e. $\zeta_0(t) = \zeta(0,t)$ is presented as a function of time. The curves corresponding to different values of D almost overlap and the small differences between them developed for $t \lesssim \tau_d$ (see the inset in Fig. 7) do not change appreciably at later times.

In order to discuss the time evolution of the interfacial apex more thoroughly we rewrite Eq.(44) for $r = 0$ in the form convenient for the analysis of the relevant time scales

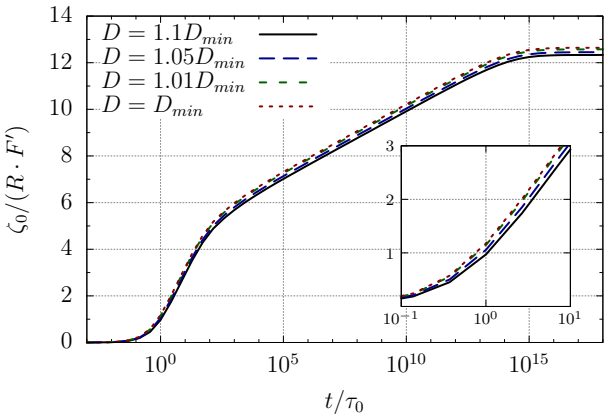

Fig. 7 Time evolution of the position of the interface's apex given by Eq.(44) and normalized by the total force F' for $H = 100R$ and different values of the distance D.

$$\zeta_0'(t') = \frac{F'}{2}\int_{-\infty}^{\infty} \frac{e^{2w}}{e^{2w}+\tilde{B}_o} e^{2w} d'^2 K_2(e^w d') \{1 - \exp[-\exp(\ln(\Gamma'(e^w)) + \ln t')]\} dw \,. \quad (46)$$

As a result, the following analytical approximation of $\zeta_0'(t')$ can be found in different time regimes

$$\zeta_0'(t') \approx F' \begin{cases} C_1 t'/d' & \text{for } t \ll \tau_d \\ \ln(t'/d') + C_2 & \text{for } \tau_d \ll t \ll \tau_H \\ \frac{1}{4}\ln(t' H'^3/d'^4) + C_3 & \text{for } \tau_H \ll t \ll \tau_\lambda \end{cases} , \quad (47)$$

where $C_1 \approx 1.178$, $C_2 \approx 0.5$, and $C_3 \approx 0.486$; see Appendix B. Fig. 8 presents the time evolution of the apex position obtained numerically for $D = 1.1D_{min}$ and $H = 1000R$. In the same figure the analytical approximations given by Eq.(47) are also presented. For such a thick film all stages of the evolution can be clearly distinguished. One can see that the approximations are very accurate except for the three transition regions near $t = \tau_d$, $t = \tau_H$, and $t = \tau_\lambda$.

In the initial stage of time evolution the apex position grows linearly with time up to $t \approx \tau_d$ which is independent of H.

In the second stage of evolution one observes the logarithmic growth of the apex position which can be well described within the infinite thickness approximation and therefore remains independent of H. This stage is bounded by $t \approx \tau_H$ and can be detected only if $H/d \gg 1$.

For $t \gg \tau_H$ the evolution of the interface is determined by the TLF dynamics. The apex position still growth logarithmically with the prefactor decreased 4 times as compared to the previous stage. The role played by the film thickness in various stages of time evolution can be seen in Fig. 9 which shows

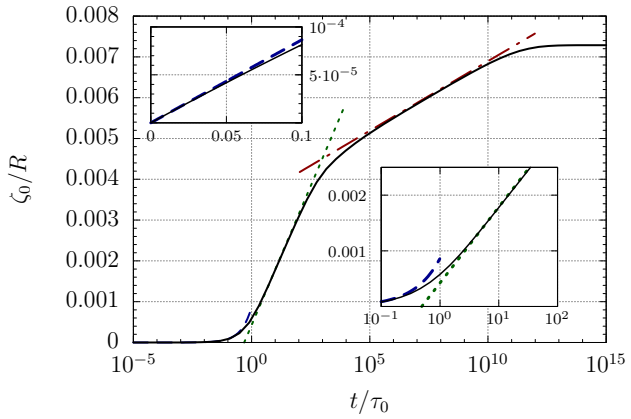

Fig. 8 The time evolution of the apex position given by Eq.(46) for $H = 1000R$ and $D = 1.1D_{min}$. The solid line describes the results of numerical integration with the general form of the decay rate given by Eq.(35) while the dotted, dashed, and dash-dotted lines represent the analytical approximations given by Eq.(47). The insets show the plots of the initial stages of evolution.

the time dependence of the apex position for $D = 1.1D_{min}$ and different values of film thickness H. First of all, the film thick-

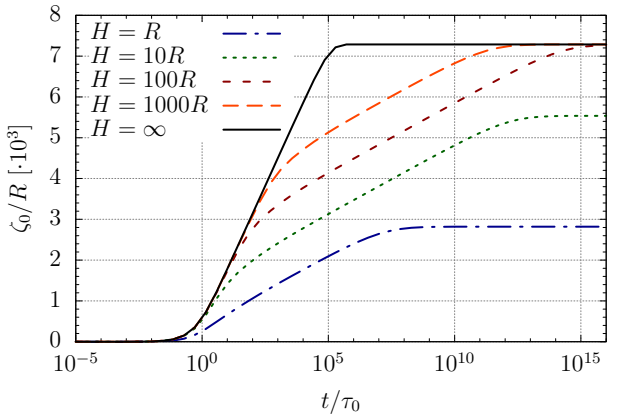

Fig. 9 The time evolution of the apex position given by Eq.(46) for $D = 1.1D_{min}$ and different values of film thickness H.

ness H influences the value of parameter τ_H and therefore determines the crossover time from the infinite thickness to the TLF dynamics. The growth rates are different in both types of dynamics and thus the overall evolution time varies with H. The time scale τ_λ also depends on H via the effective capillary length. This dependence results not only in the change of relaxation time but it also influences the equilibrium profile of the interface [15]. For very thin films both the interface deformation and the relaxation time increase with increasing H. However, while the deformation of the interface is a monotonous function of the film thickness the relaxation time

$$\tau_\lambda/\tau_0 = \left(B_o + \frac{3H_a}{8H'^4}\right)^{-2} H'^{-3} \tag{48}$$

reaches the maximum at $H'_{max} = \left(\frac{5H_a}{8B_o}\right)^{1/4}$. For the values of parameters used in our study one has $H'_{max} = 50$.

The hydrostatic pressure in the liquid film becomes relevant only for $r \gtrsim \lambda$ [13,14]. At smaller distances, it is the mean curvature of the interface which is the relevant variable. Therefore it is interesting to look at the time evolution of this quantity. The dimensionless curvature of the interface at its apex

$$2\kappa'_0 = 2R\kappa_0 \approx -\left(\frac{\partial^2\zeta'}{\partial r'^2} + \frac{1}{r'}\frac{\partial\zeta'}{\partial r'}\right)_{r'=0} = -2\frac{\partial^2\zeta'}{\partial r'^2}\bigg|_{r'=0}. \tag{49}$$

can be approximated as

$$|\kappa'_0| \approx \frac{F'}{4}\int_{-\infty}^{\infty} e^{4w} d^2 K_2(e^w d) \{1 - \exp[-\exp(\ln(\Gamma(e^w)) + \ln t')]\}\mathrm{d}w\,. \tag{50}$$

One concludes that the small wave numbers $k \ll 1$ are exponentially damped and thus are not relevant for the evolution of the curvature at the apex. Therefore, for $H > R$ the infinite thickness approximation can be used to obtain

$$|\kappa'_0| \approx \frac{F'}{4d'^2}\int_{-\infty}^{\infty} e^{4w} K_2(e^w) \{1 - \exp[-0.5\exp(w + \ln(t'/d'))]\}\mathrm{d}w\,. \tag{51}$$

As one could expect the apex curvature depends neither on the Bond number nor the film thickness but is sensitive to details of the interaction between the liquid and the probe. The results of numerical evaluation of the integral in Eq.(50) are presented in Fig. 10.

The curvature equilibrates at time $t \sim \tau_d$, which weakly depends on D but nevertheless remains close to the time τ_R presented in Fig. 10. Consequently, the relaxation time of the curvature is is much smaller than the relaxation time for the whole deformation process. This observation will prove relevant for the analysis of time dependent perturbations. In particular, if the disjoining pressure varies on a time scale much larger than τ_R then the curvature at the apex can be considered as equilibrated during the whole time evolution of the interface.

3.2 A point-force approximation

In previous sections we showed that the deformation of the interface is, to a large extent, independent of the details of the disjoining pressure Π_p and is rather determined by the total

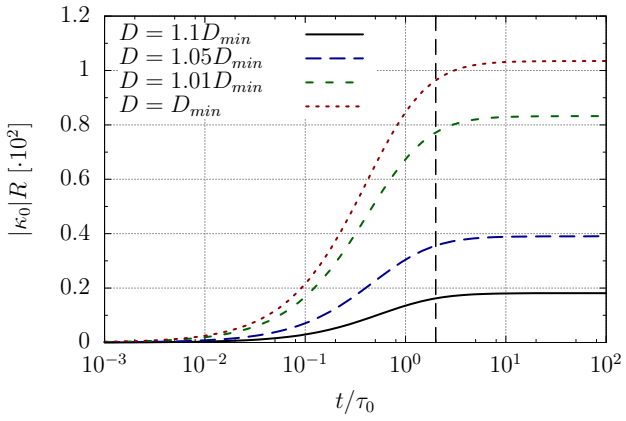

Fig. 10 The time evolution of the apex curvature, Eq.(50), for different values of the distance D. The dashed vertical line denotes the position of $t = \tau_R$.

force exerted on the surface of liquid. In this section we use this observation to discuss the evolution of the interface under the influence of a time-dependent perturbation.

Our analysis is based on Eq.(36) with the initial condition $\zeta(r,t=0)=0$. The integrand in the second term on the rhs is represented as a product of factors. Each of them refers to a different aspect of the liquid film dynamics. The forcing term $\hat{\Pi}_p(k,t-\tau)$ describes the amount of energy inserted into various k-modes. It also determines the upper cutoff for the relevant wave numbers. In the case of the van der Waals interparticle interactions the contribution corresponding to $k \gg 1/d$ turns out to be negligible. The exponential factor describes the relaxation of different wave numbers. We have already shown that large wave numbers equilibrate faster than small ones. As a result, for $\tau \gtrsim \tau_d$ the upper cutoff is determined by the relaxation term rather than by the forcing term. In such a case one can approximate the forcing term by the total time-dependent force acting on the interface

$$\hat{\Pi}_p(k,t-\tau) \approx \hat{\Pi}_p(0,t-\tau) = -F(t-\tau). \qquad (52)$$

For $r \gg d$ this approximation becomes even better since the presence of the oscillating Bessel function reduces the contribution from large wave numbers, $k \gtrsim 1/d$.

Within the above approximation one obtains

$$\zeta'(r',t') = \int_0^{\ln t'} F'(t'-e^s)\tilde{K}_{r'}(s)\mathrm{d}s\ , \qquad (53)$$

where $s = \ln\tau' = \ln\tau/\tau_0$, and

$$\tilde{K}_{r'}(s) = \frac{e^s}{2}\int_0^\infty \frac{J_0(k'r')}{g(k'H')} e^{-\Gamma'(k')e^s}\mathrm{d}k'\ . \qquad (54)$$

is called the logarithmic response function (LRF). Its structure is determined by the relation between the length scales H, r, and λ, with the corresponding time scales τ_H, $\tau_r = \tau(1/r)$, and τ_λ. Figure 11 presents four representative shapes of the LRF for $r' = 100$, $B_o = 10^{-10}$, and different thicknesses H.

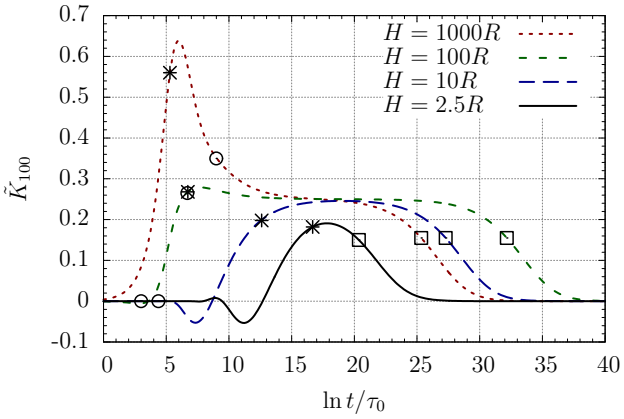

Fig. 11 The logarithmic response function $\tilde{K}_{100}(s)$ for $H' = 2.5,\ 10,\ 100,$ and 1000. Different symbols denote different time scales: (stars) τ_r, (circles) τ_H, and (squares) τ_λ.

For regions of the interface corresponding to $\tau_r \ll \tau_H$ the response to the perturbation is negligible at short times $\tau \ll \tau_r$. On the other hand it increases significantly in the vicinity of τ_r reaching the maximum, which - upon increasing H - turns into a plateau with the value 1.

When the time τ_H is approached the value of the LRF decreases, which is related to transition from the infinite thickness to the TLF dynamics. For $\tau_H \ll \tau \ll \tau_\lambda$ another plateau turns up, with the value 0.25. This constant-response region is limited by $\tau \sim \tau_\lambda$ beyond which the LRF finally vanishes.

For $r \sim H$ the qualitative behaviour of the LRF is similar to the previously discussed case $r \ll H$ although its maximum is strongly suppressed by finite thickness of the liquid film. The value at maximum is close to the values corresponding to time scales τ_r and τ_H. Consequently, only the initial stage of the temporal response of the interface is governed by the infinite thickness approximation.

In the region $r \gg H$ one has $\tau_H \ll \tau_r$ and thus the LRF is completely described by the TLF approximation. In this case one observes strong negative response of the interface before the actual relaxation process takes place. This is a characteristic feature of the TLF dynamics. Since the transport of the liquid from remote regions is much suppressed by the viscous drag, any increase of the film thickness in a given region is correlated with its depletion in the neighbouring rim, which in turn induces subsequent bumps and depletion regions at more distant regions of the interface. The magnitude of these oscillations decreases rapidly with the distance from the perturbing object and usually only the first negative-response region can be distinguished. This effect is particularly important in the

dewetting phenomena, where it can cause secondary instabilities of the liquid film[24].

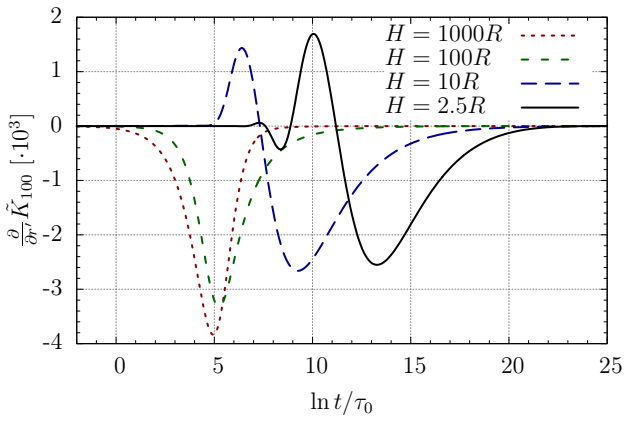

Fig. 12 Derivative of the LRF $\partial\tilde{K}_{100}/\partial r'(s)$ for $H' = 2.5,\ 10,\ 100,$ and 1000.

The relaxation time τ_{r_0} separates two different types of the response of the interface at $r \sim r_0$, to the perturbing force. For $\tau \lesssim \tau_{r_0}$ the actual relaxation process takes place. At this stage a local shape of the interface evolves. This can be seen in Fig. 12, where we present the LRF corresponding to the interfacial slope $\partial\zeta'/\partial r'$. It is given by $\partial\tilde{K}_{r'}(s)/\partial r'$. One observes that the time window in which the action of the force influences the local shape of the interface is located at $\tau \lesssim \tau_{r_0}$, and decays quickly for $\tau > \tau_{r_0}$. At larger times modification of the interface position at $r \lesssim r_0$ is related to the deformation of the interface at larger separations from the perturbing sphere. We have already observed this effect in the case of constant force when the inner part of the profile preserved its shape during the whole evolution of the interface. One concludes that if the time-varying force is approximately constant on time scales shorter than τ_{r_0} then the region of interface corresponding to $r \lesssim r_0$ remains always in mechanical equilibrium with the current value of the force.

In the case of constant force the constant-response region of the LRF for $t \gg \tau_H$ leads to the logarithmic growth of the interface

$$\zeta'(r',t') = F' \cdot \left(\frac{1}{4}\ln t' + C(r,H,\tilde{B}_o)\right) , \qquad (55)$$

where the time independent function C has to be derived from the response function. It can be done using the following property

$$\int_{-\infty}^{\infty} \tilde{K}_{r'}(s)\mathrm{d}s = K_0(\tilde{B_o}^{1/2} r') , \qquad (56)$$

where K_0 denotes the zeroth-order modified Bessel function of the second kind. Consequently, one can show that for $r \ll \lambda$

$$C(r,H,\tilde{B_o}) \approx \frac{1}{4}\ln\left(\frac{H'^3}{r'^4}\right) - 0.014 , \qquad (57)$$

see Appendix C for details.

3.3 Scaling of the response function

Although the integral in the expression defining $\tilde{K}_{r'}(s)$, see Eq.(54), cannot be calculated analytically in the general case, one can discuss its asymptotic behaviour and scaling properties. For $\tau \ll \tau_\lambda$, the rescaling of both position $\tilde{r} = r/H$ and time $\tilde{\tau} = \tau'/H' = \tau/\tau_0 \cdot R/H$ gives

$$\tilde{K}_{\tilde{r}}(\tilde{s}) = \frac{e^{\tilde{s}}}{2}\int_0^\infty \frac{J_0(k'\tilde{r})}{g(k')} e^{-\frac{k'}{2g(k')}e^{\tilde{s}}}\mathrm{d}k' , \qquad (58)$$

where $\tilde{s} = \ln(\tau'/H')$. Further simplifications can be made both within the TLF and the infinite thickness approximations. For $\tau \ll \tau_H$ the response function takes the form

$$\tilde{K}_{\tilde{r}}(\tilde{s}) = \mathscr{Q}\left(\frac{e^{\tilde{s}}}{2\tilde{r}}\right) - e^{\tilde{s}}\mathscr{R}\left(\frac{1}{\tilde{r}}\right) , \qquad (59)$$

where

$$\mathscr{Q}(x) = \int_0^\infty e^{-w} J_0\left(\frac{w}{x}\right)\mathrm{d}w , \qquad (60)$$

and

$$\mathscr{R}(x) = \int_0^\infty \left(1 - \frac{1}{g(w)}\right) J_0\left(\frac{w}{x}\right)\mathrm{d}w . \qquad (61)$$

The function $e^{\tilde{s}}\mathscr{R}(1/\tilde{r})$ can be interpreted as a correction to the infinite thickness approximation due to a finite thickness of the liquid film and it vanishes for infinitely thick films.

On the other hand, for $\tau_H \ll \tau \ll \tau_\lambda$ one has

$$\tilde{K}_{\tilde{r}}(\tilde{s}) = \frac{1}{4}\mathscr{P}\left(\frac{e^{\tilde{s}}}{3\tilde{r}^4}\right) , \qquad (62)$$

where

$$\mathscr{P}(x) = \int_0^\infty e^{-w} J_0((w/x)^{1/4})\mathrm{d}w . \qquad (63)$$

For $\tau \gg \tau_\lambda$ the decay rate can be approximated by

$$\tilde{K}_{r'}(s) = \frac{3\tilde{B_o}^2}{H'^3} e^{-s} . \qquad (64)$$

This asymptotic scaling shows that in the final stage of the interface evolution the equilibrium deformation profile is approached according to the power law $\zeta_{eq}(r) - \zeta(r,t) \propto 1/t$.

The scaling functions $\mathscr{P}, \mathscr{Q}$ and $\mathscr{R}$ are shown in Fig. 13. One concludes that $x \sim 1$ at which the functions $\mathscr{P}$ and $\mathscr{Q}$ reach the asymptotic plateau is related to the relaxation time τ_r

$$\tau_r \approx \begin{cases} 2r'\tau_0 & \text{for } r' \ll H' \\ \frac{3r'^4}{H'^3}\tau_0 & \text{for } r' \gg H' \end{cases} . \qquad (65)$$

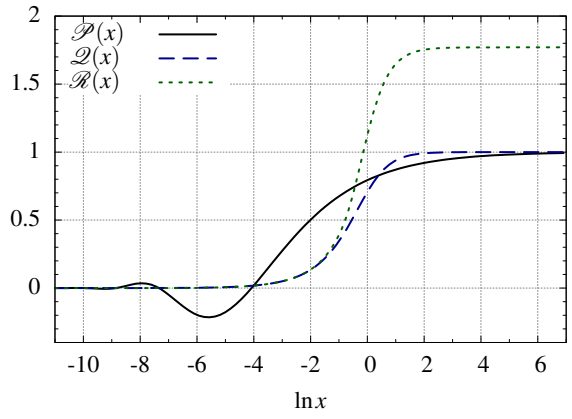

Fig. 13 The scaling functions $\mathscr{P}$, $\mathscr{Q}$, and $\mathscr{R}$.

As we have already shown this is a relevant time scale, which separates two different types of the interface response to the perturbing force.

3.4 Response to a periodic perturbation

In principle, Eq.(53) provides a tool for calculating the deformation of the interface for a given time-dependent perturbation. If the force is known *á priori* the integral can be explicitly evaluated. For example, this is the case of a vertically oscillating AFM probe, provided the deformation of the interface is negligible compared to the separation between the probe and the interface. This problem was analysed by Ledesma-Alonso et al.[20] for thin liquid films. In this section we investigate how the behaviour of the interface changes upon increasing H and going beyond the regime of validity of the TLF approximation used in Ledesma-Alonso et al.[20]. We will show that restricting the analysis to the lubrication approximation may lead to noticeable inaccuracy in predictions concerning the position of the interface even for relatively thin films.

We consider the case of an oscillating sphere with

$$D(t) = D_0 + A\cos\omega_0 t \ , \tag{66}$$

where D_0 is the mean distance between the probe and the interface, and A is the amplitude of oscillations. Consequently, the dimensionless total force exerted on the interface is given by

$$F'(t) = \frac{H_a}{4(D'(t)^2-1)^2} \ . \tag{67}$$

The results presented below have been obtained for the following set of parameters

$$H_a = 10^{-3}, \qquad B_o = 10^{-10},$$
$$D_0 = 1.3\cdot D_{min}, \qquad A = 0.29\cdot D_{min} \ .$$

Figure 14 shows the time evolution of the interface evaluated at $r = 2R$ during the tenth period of force oscillations for $T_0 = 2\pi/\omega_0 = 100\tau_0$ and different values of H. The curves were obtained using three different methods: the direct solution of the TLF equation (see Appendix D), the integration of the LRF within the TLF approximation, and the integration of the general form of the LRF.

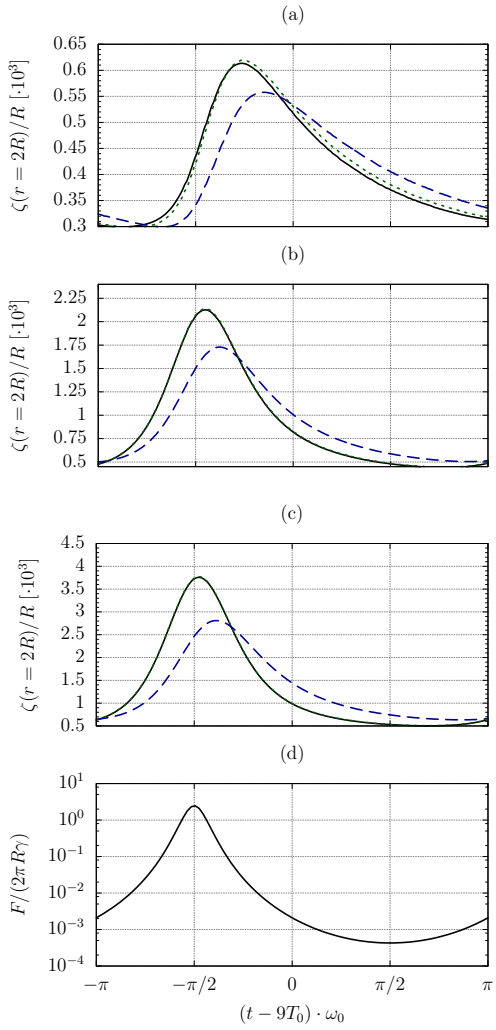

Fig. 14 The time evolution of the interface evaluated at $r = 2R$ for $T_0 = 100\tau_0$ and different thicknesses of the liquid film: (a) $H = R$, (b) $H = 5R$, (c) $H = 20R$. Different lines correspond to different methods used to obtain these results: the numerical solution of the TLF equation (solid line), the integration of the LRF within the TLF approximation (dotted line), and the integration of the general form of the LRF (dashed line). The plot (d) shows the time evolution of the force acting on the interface.

In Fig. 14a all three curves are close to each other. One observes a small difference between the direct solution of

the TLF equation and the method using the LRF within the TLF approximation. This difference is the consequence of the point-force approximation used in the derivation of the LRF. The point $r = 2R$ is relatively close to the apex and such small deviations from the solution obtained for the exact profile of the disjoining pressure can be expected. On the other hand, the dashed line representing results based on the general form of the LRF differs from the two other lines in a more pronounced way. This indicates a rather limited applicability of the TLF approximation for this system. For $H = R$ the deformation of the interface in the vicinity of the apex is determined by the wave numbers $k \gtrsim 1/H$ whose relaxation cannot be fully described by the TLF approximation. Here, the short-time evolution corresponds to the transition region between the infinite thickness and the TLF dynamics. This effect becomes more evident for thicker films. One notes that in these cases (e.g., $H = 5R$ and $H = 20R$) the general LRF method predicts smaller deformation than the TLF approximation does. Another difference between these two approaches is the phase shift[20], i.e., the shift between the maximum of the deformation and the maximum of the force †. For increasing thickness of the film the phase shift calculated within the TLF approximation decreases and the response of the interface is almost quasi-static for $H = 20R$. This is related to a strong decrease of the relaxation time $\tau_r \propto H^{-3}$, which implies that a large part of the interface remains in mechanical equilibrium with the force acting on the interface. According to the general dispersion relation the relaxation time becomes independent of H for thick films and thus one observes only a small decrease of the phase shift in this case. This is also the reason for larger values of the interface deformation obtained within the TLF approximation. Underestimation of the relaxation time causes a faster response of the interface which leads to larger deformations when the force is maximal.

If we look at the deformation of the interface at the time scale of a single period, all differences between different types of dynamics that are present on time scales much shorter than T_0, can be disregarded. In particular, for oscillations with the period $T_0 \gg \tau_H$ the TLF approximation can be successfully used to describe the dynamics of the interface even though it is not adequate for a short time evolution of the apex region. This is presented in Fig. 15, where the time evolution of the interface evaluated at $r = 2R$ is shown for $H = 5R$ and different values of the period T_0. In this system one has $\tau_H = 40\tau_0$. For $T_0 = 1000\tau_0$ the time evolution of the interface is governed by the TLF approximation. However, upon increasing the oscillations frequency the TLF approximation leads to growing deviations from the results obtained within the general form of the LRF.

For large frequencies of the perturbation the dynamics of the inner part of the interface around the apex can be very important, in particular when one analyses a jump-to-contact phenomenon, which is governed by instability in the region of large wave numbers[20]. Our results show that for such cases it may be essential to use the general form of the dispersion relation presented in this study, even for relatively thin films.

† Note that Ledesma-Alonso et al.[20] used slightly different definition of the phase shift.

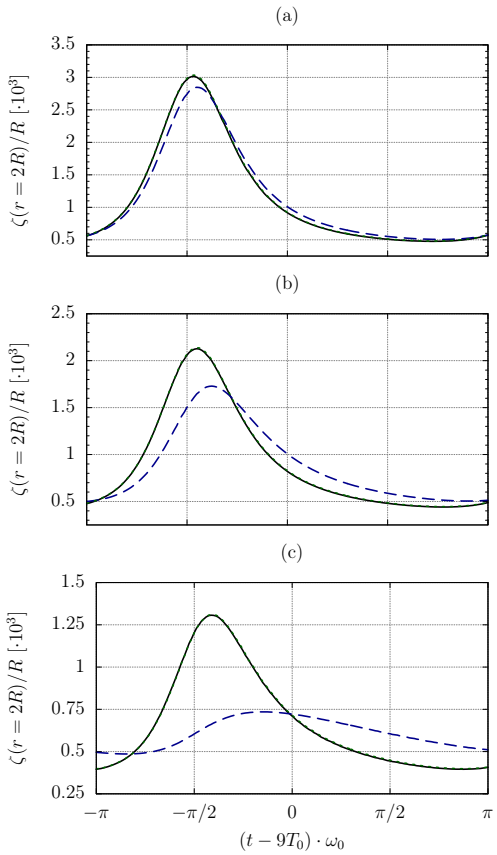

Fig. 15 Time evolution of the interface position at $r = 2R$ for $H = 5R$ and different periods T_0 of the force oscillations: (a) $T_0 = 1000\tau_0$, (b) $T_0 = 100\tau_0$, (c) $T_0 = 10\tau_0$. The line styles are the same as in Fig. 14

4 Conclusions

In this study we analysed the dynamics of a liquid film of arbitrary thickness. The deformation of the liquid–gas interface was caused by its interaction with the AFM tip modeled by a nano-sized sphere. In the first part, we studied the time evolution of an initially planar interface towards the non-planar equilibrium configuration. In order to be able to consider liquid films of arbitrary thickness we based our analysis on the general dispersion relation[31] in the limit of small values

of parameter $\omega/\nu k^2$ which can be interpreted as k-dependent Reynolds number. We derived the relevant length and time scales and discussed their role in the dynamics of the interface deformation. In particular, we identified the time scale τ_H which separates the regimes governed by two different forms of the asymptotic dynamics: one corresponds to the infinite thickness approximation and the other to the TLF approximations. It turns out that due to the multi-scale character of the interface deformations usually each approximation becomes relevant in the appropriate regime in which it explains different aspects of the interface dynamics. In the special case of a constant force acting on the interface we obtained analytical expressions describing approximately the time evolution of the interface and - upon comparison with the numerical results - we checked that these expressions provide a reliable description of dynamics.

We showed that if the interface is perturbed by a small object both the equilibrium and the transient profiles can be to a large extent described by a point-force approximation. Deviations from this approximation are essential only in the vicinity of the apex and for very short times. This observation allowed us to derive the response function for the deformation of the interface perturbed by a time-dependent force. The response function for a point at the interface can be characterized by three different time scales which are related to the relevant length scales: the lateral distance from the AFM tip, the thickness of the liquid film, and the so-called effective capillary length. The response function shows different scaling behaviour in different time regimes and we discussed the corresponding analytical approximations. The response function method can prove useful in bridging the inner and outer solutions in multiscale simulations [18].

In the second part we discussed the response of the interface to the action of the oscillating perturbation. Similar problem has been extensively studied by Ledesma-Alonso et al. [20] within the TLF approximation. Our analysis is valid for arbitrary film thickness. We showed that in the vicinity of the apex the interface evolution is strongly influenced by the finite thickness of the film even for relatively thin films. This effect is more significant for larger frequencies of force oscillations and can be neglected for the oscillation periods much larger than the time scale τ_H.

The important aspect of many AFM experiments is the so–called jump-to-contact phenomenon which is related to large wave numbers instability [20]. It may prove interesting to study its occurrence and characteristics within an approach which goes beyond the TLF approximation. One of the issues is to see how the minimum distance between the tip and the liquid-gas interface depends on the film thickness and the frequency of the tip oscillations. This is an important question, since in many AFM experiments the so-called zero distance, i.e. the position of the unperturbed liquid-gas interface, is approximated by the elevation of the AFM tip at the moment of the capillary bridge formation [2]. Our results can also prove relevant when studying dynamics of mircon-sized droplets which can hardly be described within the TLF approximation.

In this paper we provided a general framework for description of the liquid film dynamics. The proposed method can be applied to different systems characterised by various length and time scales, as well as by different forms of the disjoining pressure. We showed the capacity of the method in the case of simple van der Waals interactions in the mean field approximation. In addition, most of our results were presented for the linearised form of the disjoining pressure. These simplifications allowed for a transparent description of the important features of the liquid film dynamics. However, they also imply that the numerical values of parameters presented in the text need to be applied with caution. Weak perturbation represented by the linearised disjoining pressure gives rise to relatively small deformations of the interface. Their magnitude is comparable to the molecular size for small radii of the perturbing sphere. On one hand such small deformations are hardly accessible experimentally and the hydrodynamic description turns out inaccurate, although the hydrodynamic equations have already been successfully used down to the scale of a nanometer [24]. On the other hand, the deformation of the interface increases when the full form of the disjoining pressure is considered, e.g. in the description of the jump-to-contact phenomena. Numerical solutions to Eq.(33) with the nonlinear disjoining pressure can be obtained with the help of the Hankel transform method presented in Ledesma-Alonso et al. [20]. Also for larger sizes of the perturbing object the resulting deformations can be reliably captured by the continuum models.

The complete description of small systems ($\sim$ 10 - 100 nm) at room temperatures should take into account thermal fluctuations. In particular, one may consider using the form of the disjoining pressure obtained within the renormalization group approach [27] or incorporate the stochastic tensor into the hydrodynamic equations [35]. Also, in real systems other types of interaction may occur, e.g. electrostatic. They would influence the deformation height but not the general aspects of the liquid film dynamics encoded in the dispersion relation and discussed in the paper.

Since our method is based on the linearised Navier-Stokes equations in the limit of small Reynolds numbers, one can expect it to fail when the inertia of the liquid becomes relevant. Our model needs to be applied with caution also when the deformation of the interface is comparable with the thickness of the film or the slope of the interface becomes too big. In such cases numerical solution of the Stokes equation may be the only option.

A Boundary conditions

The derivation of the dispersion relation, see Eqs (24) and (31), is based on standard boundary conditions for incompressible, viscous liquid. However, for various micro- and nanoscale systems one can contemplate using different forms of boundary conditions. In particular, it has been observed that liquid may experience slip at a substrate-liquid interface[24]. To include this effect in theoretical analysis the so-called Navier boundary conditions can be introduced at the substrate-liquid interface

$$(u_x,u_y) = b\frac{\partial(u_x,u_y)}{\partial z} \quad \text{at } z=0\,, \tag{68}$$

where the parameter b is called the slip length. Consequently a modified form of the dispersion relation is obtained. In the limit $\omega/\nu k^2 \ll 1$ it differs from that presented in Eq.(31) by the modified form of the function $g(kH)$. In the partial-slip case it depends additionally on the slip length b and has the following form

$$g(k,H,b) = \frac{\cosh^2(kH)+(kH)^2+2kb(kH+\sinh(kH)\cosh(kH))}{\sinh(x)\cosh(x)-x+2kb\sinh^2(kH)}\,. \tag{69}$$

In general, the presence of a partial slip decreases the characteristic time scales governing the liquid film dynamics. On the other hand it does not change the qualitative behaviour of the dispersion relation, which agrees with the results obtained for thin liquid films[24].

Chan et al.[18] showed that in many cases liquid-gas or liquid-liquid interfaces may exhibit an immobile behaviour in contrast with the stress continuity condition. It results in a no-slip boundary condition at the free surface and thus decouples the shear stresses in fluids on either side of the interface. Consequently, the function $g(kH)$ takes the following form

$$g(kH) = \frac{\sinh(kH)\cosh(kH)+kH}{\sinh^2(kH)-(kH)^2}\,. \tag{70}$$

The detailed analysis of the influence of the above modified dispersion relations on the dynamics of our system is beyond the scope of this paper.

B Derivation of analytical approximation to the evolution of the apex position

The integrand in Eq.(46) can be split into three factors

$$\zeta_0'(t') = \frac{H_a}{4d'^4}\int_{-\infty}^{\infty} p(w)\,q(w)\,z(w)\mathrm{d}w \quad , \tag{71}$$

where $p(w) = e^{2w}/(e^{2w}+\tilde{B}_o)$, $q(w) = e^{2w}d^2K_2(e^w d)/2$, and $z(w) = 1-\exp[-\exp(\ln(\Gamma(e^w))+\ln t')]$. All the functions $p,q,$ and z have sigmoidal shape and are presented in Fig. 16. The transition regions of functions p and q are given by $w \approx w_p = 0.5\ln\tilde{B}_o$ and $w \approx w_q = -\ln d'$, respectively. The position of the transition region for the function z depends on t' and H' (via Γ). For $t \ll \tau_H$ one has $w_z = \ln(t'/2)$ and for $t \gg \tau_H$ one obtains $w_z = 1/4\ln(t'H'^3/3)$; in consequence $w_z > w_p$ for $t < \tau_\lambda$. Moreover, if the scales set by w_p, w_q, and w_z are well separated then one can use the following approximation

$$\begin{aligned}\zeta_0'(t') \approx \lim_{\varepsilon_1,\varepsilon_2\to\infty}\frac{H_a}{4d'^4}\Bigg[\int_{-\infty}^{w_z+\varepsilon_1} z(w)\mathrm{d}w + \\ +\int_{w_z+\varepsilon_1}^{w_q-\varepsilon_2}\mathrm{d}w+\int_{w_q-\varepsilon_2}^{\infty} q(w)\mathrm{d}w\Bigg] = \\ =\frac{H_a}{4d'^4}\left[w_q-w_z+C\right]\,,\end{aligned} \tag{72}$$

where the constant C is given by

$$C = \lim_{\varepsilon_1,\varepsilon_2\to\infty}\int_{-\infty}^{w_z+\varepsilon_1} z(w)\mathrm{d}w-\varepsilon_1+\varepsilon_2+\int_{w_q-\varepsilon_2}^{\infty} q(w)\mathrm{d}w\,. \tag{73}$$

It can be shown that C depends neither on $d',H',\tilde{B}_o$ nor t'. However, it does depend on the form of the decay rate present in function $z(w)$ and it matters whether we use the infinite thickness or the TLF approximation.

On the other hand, for $t \ll \tau_d$ transition regions of $q(w)$ and $z(w)$ overlap while the function $z(w)$ can be approximated by

$$z(w) \approx \frac{t'}{2}\exp(w)\,. \tag{74}$$

This gives the linear growth of the apex position in the initial stage of time evolution

$$\zeta_0'(t') \approx \frac{H_a}{4d'^4}\frac{t'}{2d'}\int_{-\infty}^{\infty} e^{3w}K_2(e^w)\mathrm{d}w\,. \tag{75}$$

C Derivation of the constant $C(r,H,\tilde{B}_o)$

In the regime of constant response, i.e., for $\tau_r,\tau_H \ll t \ll \tau_\lambda$ the deformation of the interface under influence of a constant force F' can be written as

$$\begin{aligned}\zeta'(r',t') = F'\int_{-\infty}^{\ln t'}\tilde{K}_{r'}(s)\mathrm{d}s = \\ F'\left[\int_{-\infty}^{x}\tilde{K}_{r'}(s)\mathrm{d}s-\frac{1}{4}x+\frac{1}{4}\ln t'\right]\,,\end{aligned} \tag{76}$$

where x is an arbitrary parameter which lies in the constant response region and the lhs does not depend on x. Using Eq.(55) one can identify the function $C(r,H,\tilde{B}_o)$ as

$$C(r,H,\tilde{B}_o) = \int_{-\infty}^{x}\tilde{K}_{r'}(s)\mathrm{d}s-\frac{1}{4}x\,, \tag{77}$$

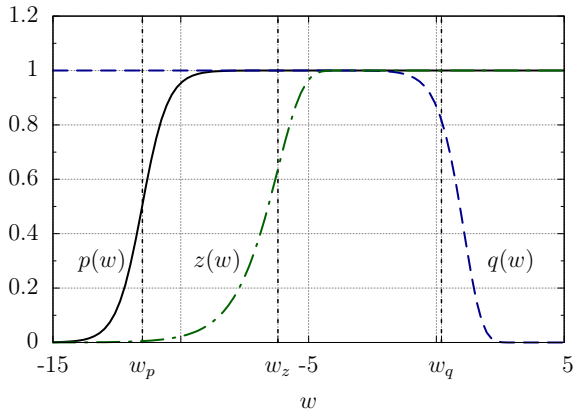

Fig. 16 Different parts of the integrand in Eq.(71) evaluated for $\tilde{B}_o = 10^{-10}$.

which should not depend on the choice of x. Using the result from Eq.(56) one has

$$K_0\left(\tilde{B_o}^{1/2} r\right) = C(r, H, \tilde{B_o}) + \frac{1}{4}x + \int_x^\infty \tilde{K}_{r'}(s)\mathrm{d}s \,. \qquad (78)$$

Since $\tau_r, \tau_H \ll e^x$ one can use the TLF approximation to get

$$\int_x^\infty \tilde{K}_{r'}(s)\mathrm{d}s = \int_0^\infty \frac{k'}{k'^2 + \tilde{B_o}} e^{-\frac{1}{3}(k'H')^3 (k' + \tilde{B_o}/k') e^x} \mathrm{d}k' \quad . \quad (79)$$

Thus one obtains

$$\begin{aligned} &\int_x^\infty \tilde{K}_{r'}(s)\mathrm{d}s + \frac{1}{4}x = \\ &= \lim_{z\to-\infty} \int_0^\infty \frac{w}{w^2+1} e^{-w^2(w^2+1)e^z} \mathrm{d}w + \frac{1}{4}z + \frac{1}{4}\ln\tau_\lambda \approx \\ &\approx -\frac{1}{4}\ln\left(\tilde{B_o}^2 H'^3\right) + 0.130 \,. \end{aligned} \qquad (80)$$

Finally, the function C takes the following form

$$\begin{aligned} &C(r', H', \tilde{B_o}) \approx K_0\left(\tilde{B_0}^{1/2} r\right) + \frac{1}{4}\ln\left(\tilde{B_o}^2 H'^3\right) - 0.130 \approx \\ &\approx \frac{1}{4}\ln\frac{H'^3}{r'^4} - 0.014 \,, \end{aligned} \qquad (81)$$

where we used the asymptotic expansion of the Bessel function K_0 for a small argument, $K_0(x) \approx -\ln x + \ln 2 - \gamma$, and γ denotes the Euler-Mascheroni constant.

D The thin liquid film equation

Using the dimensionless variables introduced in Sec. 2.2 the TLF equation[33] can be written in cylindrical symmetry as follows

$$\begin{aligned} \frac{\partial \zeta'}{\partial t'} =& \frac{1}{r'}\frac{\partial}{\partial r'}\left[r' \frac{(H'+\zeta')^3}{3} \frac{\partial}{\partial r'} \right. \\ & \left. \left(-\frac{\partial^2 \zeta'}{\partial r'^2} - \frac{1}{r'}\frac{\partial \zeta'}{\partial r'} + \tilde{B}_o \zeta' + \Pi'_p \right) \right] . \end{aligned} \qquad (82)$$

The numerical solution of this nonlinear equation requires stable methods due to its high stiffness. We use an implicit finite difference numerical scheme based on the model proposed in Diez et al.[36]. The solver was implemented in the Octave environment[34]. Variable grid spacing and time stepping have been used to perform the effective numerical simulation.

Acknowledgments

K.W. acknowledges the support by the Foundation for Polish Science International PhD Projects Programme co-financed by the EU European Regional Development Fund.

References

1 J. Israelachvili, Y. Min, M. Akbulut, A. Alig, G. Carver, W. Greene, K. Kristiansen, E. Meyer, N. Pesika, K. Rosenberg and H. Zeng, *Rep. Prog. Phys*, 2010, **73**, 036601.
2 H.-J. Butt, B. Capella and M. Kappl, *Surf. Sci. Rep.*, 2005, **59**, 1–152.
3 K. A. Brown, D. J. Eichelsdoerfer, X. Liao, S. He and C. A. Mirkin, *Front. Physics*, 2013, **9**, 385–397.
4 J. Tamayo and R. Garcia, *Langmuir*, 1996, **12**, 4430.
5 T. Farhan, O. Azzaroni and W. T. S. Huck, *Soft Matter*, 2005, **1**, 66–68.
6 A. Alessandrini and P. Facci, *Soft Matter*, 2014, **10**, 7145–7164.
7 J. Jang, C. Schatz and M. A. Ratner, *J. Chem. Phys*, 2004, **120**, 1157.
8 E. Sahagun, P. Garcia-Mochales, G. M. Sacha and J. J. Saenzi, *Phys. Rev. Lett.*, 2007, **98**, 176106.
9 D. L. Sedin and K. L. Rowlen, *Anal. Chem*, 2000, **72**, 2183–2189.
10 B. L. Weeks and J. J. DeYereo, *J. Phys. Chem. B*, 2006, **110**, 10231–10233.
11 Z. Wei and Y.-P. Zhao, *J. Phys. D: Appl. Phys.*, 2007, **40**, 4368–4375.
12 R. Ledesma-Alonso, D. Legendre and P. Tordjeman, *Phys. Rev. Lett.*, 2012, **108**, 106104.
13 R. Ledesma-Alonso, P. Tordjeman and D. Legendre, *Phys. Rev. E*, 2012, **85**, 061602.
14 D. B. Quinn, J. Feng and H. A. Stone, *Langmuir*, 2013, **29**, 1427–1434.
15 R. Ledesma-Alonso, D. Legendre and P. Tordjeman, *Langmuir*, 2013, **29**, 7749.
16 R. R. Dagastine and L. R. White, *J. Colloid Interface Sci.*, 2002, **247**, 310–320.
17 S. J. Miklavcic and L. R. White, *Langmuir*, 2006, **22**, 6961–6968.
18 D. Y. C. Chan, E. Klaseboer and R. Manica, *Soft Matter*, 2011, **7**, 2235–2264.
19 Y. Z. Wang, B. Wang, X. M. Xiong and J. X. Zhang, *Surf. Sci.*, 2011, **604**, 528–538.
20 R. Ledesma-Alonso, P. Tordjeman and D. Legendre, *Soft Matter*, 2014, **10**, 7736–7752.
21 L. Jing, Z. Zhi-Jun, Y. Ji-Lin and B. Yi-Long, *Chin. Phys. Lett.*, 2009, **26**, 086802.
22 R. García and R. Pérez, *Surf. Sci. Rep.*, 2002, **47**, 197–301.
23 S. Dietrich and M. Napiórkowski, *Phys. Rev. A*, 1991, **43**, 1861–1885.

24 M. Rauscher and S. Dietrich, in *Handbook of Nanophysics: Principles and Methods*, ed. K. D. Sattler, CRC Press, 2010, ch. Nanofluidics of Thin Liquid Films.

25 S. Dietrich, M. Rausher and M. Napiórkowski, in *Nanoscale Liquid Interfaces*, ed. T. Ondarcuhu and J.-P. Aimé, Pan Stanford Publishing, 2013, ch. 3. Wetting Phenomena at Nanometer Scale, p. 83.

26 P. Jakubczyk, *Phys. Rev. E*, 2011, **84**, 021124.

27 T. Bickel, *Europhys. Lett.*, 2014, **106**, 16004.

28 J. Israelachvili, *Intermolecular and Surface Forces*, Elsevier, Amsterdam, 2011.

29 H. Lamb, *Hydrodynamics*, Cambridge University Press, 6th edn, 1994.

30 J. Lighthill, *Waves in fluids*, Cambridge University Press, 2001.

31 K. Wędołowski and M. Napiórkowski, *Phys. Rev. E*, 2013, **83**, 043014.

32 F. Closa, A. D. Chepelianskii and E. Raphaël, *Phys. Fluids*, 2010, **22**, 052107.

33 A. Oron, S. H. Davis and S. G. Bankoff, *Rev. Mod. Phys.*, 1997, **69**, 931–980.

34 J. W. Eaton, D. Bateman and S. Hauberg, *GNU Octave version 3.0.1 manual: a high-level interactive language for numerical computations*, CreateSpace Independent Publishing Platform, 2009.

35 G. Grün, K. R. Mecke and M. Rauscher, *J. Stat. Phys.*, 2006, **122**, 1261–1291.

36 J. A. Diez and K. L., *J.Comp.Phys.*, 2002, **183**, 274–306.

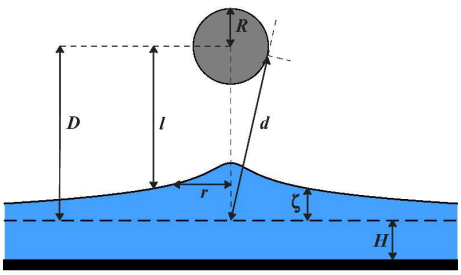

Liquid film dynamics is studied within a general theoretical framework provided for liquid films of arbitrary thickness.